(1961)].
[5]K. R. Atkins and Y. Narahara, Can. J. Phys. 33, 49 (1955).
[6]D. R. Lovejoy, Can. J. Phys. 33, 49 (1955).
[7]W. Brouwer and R. K. Pathria, unpublished.
[8]G. N. Antonov, J. Chim. Phys. 5, 372 (1907).
[9]R. Defay, I. Prigogene, A. Bellemans, D. H. Everett, Surface Tension and Adsorption (Longmans, Green and Co. Ltd., London, 1966), p. 294.
[10]J. C. Wheatley, Am. J. Phys. 36, 181 (1968).
[11]L. M. Milne-Thomson, Theoretical Hydrodynamics (Macmillan and Co., London, 1960), p. 409.
[12]D. F. Brewer, A. J. Symonds, and A. L. Thomson, Phys. Rev. Letters 15, 182 (1965).

PHYSICAL REVIEW VOLUME 179, NUMBER 1 5 MARCH 1969

Properties of an Afterglow Helium Plasma*

J. W. Poukey, J. B. Gerardo, and M. A. Gusinow
Sandia Laboratories, Albuquerque, New Mexico
(Received 1 November 1968)

The role played by individual atomic reactions and transport processes in the decay of a helium afterglow plasma in a long cylindrical vessel is studied by solving numerically a complete set of three-temperature transport equations. Comparison with the measured decay of a laboratory afterglow shows the equations to be realistic. Reactions which are found to be particularly important in determining the decay include electron-ion recombination, metastable formation, metastable-electron and metastable-metastable collisions, resonant charge exchange, and electron-ion collisions. The room-temperature wall bounding the plasma causes spatial gradients in the densities and temperatures to evolve, resulting in appreciable thermal conduction and particle convection. The relative importance of the various reactions and processes is presented quantitatively. Conclusions are reached which apply at least semiquantitatively to any afterglow helium plasma with densities, temperatures, and geometry comparable to those studied here.

I. INTRODUCTION

The properties of a partially ionized, decaying helium plasma in an infinite cylindrical tube were studied by numerical solution of a set of transport equations. The role played in the decay by individual atomic reactions, transport processes and spatial nonuniformities of constituent parameters was investigated. Gray and Kerr[1] previously studied the spatial and temporal behavior of the electron density in a bounded plasma, but did not allow for spatial nonuniformities other than the free electron and ion densities. Considered here is the more general case in which all plasma quantities are permitted to evolve nonuniformly, and various atomic reactions and transport processes are included explicitly. The relative importance of the role played by each in governing the decay of electron density and temperature was quantitatively studied. The reactions and processes which were given major attention include: electron-ion recombination, metastable-electron and metastable-metastable collisions, thermal conduction and metastable formation.

The study was carried out for a partially ionized helium plasma with an electron temperature of a few thousand degrees, a background gas pressure of a few Torr, a degree of ionization of $< 2\%$ and contained in a long cylindrical tube with a room-temperature wall. The set of initial conditions was chosen to correspond to those of an extensively investigated laboratory plasma.[2] This permitted comparison of the theoretical plasma model with the laboratory plasma. This served to illustrate that the model is realistic. The results presented here strictly apply only to the particular plasma which served as the basis for the theoretical model. However, conclusions are drawn from this study which are applicable in part to many laboratory afterglow helium plasmas.

Convective particle flow is commonly estimated in studies of the type carried out here by inclusion of diffusion coefficients and particle gradients. This is a good approximation only if the flux is that of a minority constituent in a spatially uniform background; a condition which is not typical-

ly satisfied by a bounded plasma for which the background gas temperature is elevated above the wall temperature.[3] This problem was surmounted by inclusion of separate momentum transport equations and explicit particle flux terms. In addition, the set of transport equations was written so as to permit the attainment of unequal temperatures for electrons, ions and neutral atoms. It is demonstrated that this is necessary even though the relevant equilibration times are short compared to the duration of observation.

In Sec. II the laboratory plasma upon which the theoretical model is based is briefly discussed and some appropriate experimental results are presented. Section III includes a description of the set of transport equations and the method of solution. The main results of the study are presented in Sec. IV, including a discussion of the role which is played in the net decay by various reactions and processes. The results and conclusions are summarized in Sec. V.

II. THE LABORATORY PLASMA

The plasma model used here is based on the results of an extensively investigated laboratory plasma.[2] The details of the experiment are of minor concern in this study. It is mentioned here only as a means to show that the theoretical model is realistic. We present here only the pertinent results.

The experimental helium plasma was provided by a crow-barred discharge of a 1.0-μF capacitor through a vessel containing helium at 2.4 Torr pressure. The containing vessel was 2.2 cm in diameter and 30 cm long. The free electron density and neutral atom density were spatially and temporally resolved by means of two-wavelength laser interferometry, each laser interferometer operating in the high-sensitivity, spherical, coupled-cavity mode of operation. The electron temperature was measured by spectral line intensity techniques, including Abel inversion of the spectral lines for spatial resolution. The gas temperature was inferred from the velocity of sound in the gas.

The pertinent experimental results are shown in Figs. 1–4 and 10. The solid curves are the corresponding values for the theoretical plasma which will be fully discussed later. The indicated error bars on the experimental results are fully discussed in Ref. 2.

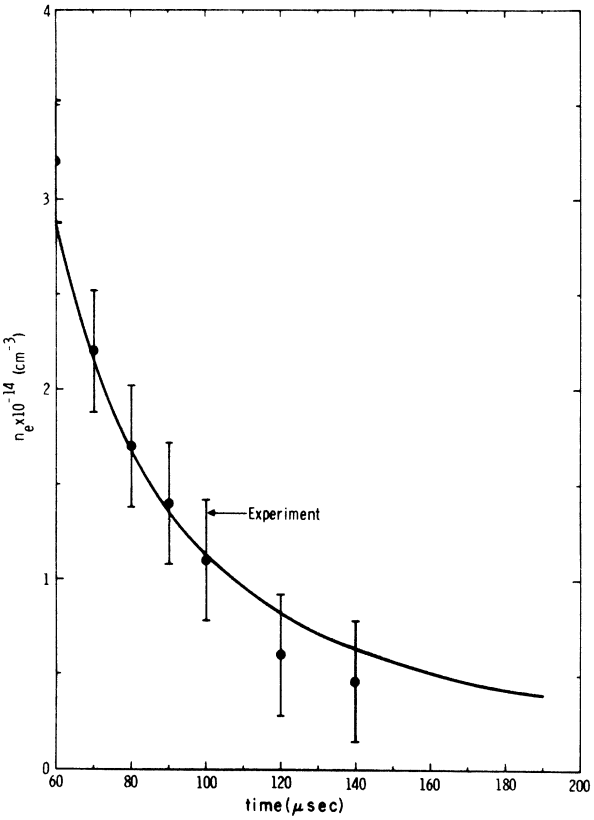

FIG. 1. Electron density on axis versus time. The solid curve represents the results of the reference run. The data points and error flags illustrate the experimental results.

III. THEORY

A. Equations

A set of equations suitable for describing the macroscopic behavior of a bounded helium afterglow plasma is presented in this section. Temperatures of a few thousand degrees are considered with neutral atom densities on the order of 10^{16} cm^{-3}, and a degree of ionization on the order of 1%. The following notation is used for the sth species of particles: n_s is number density, T_s is temperature, $\vec{v}_s$ is average velocity, m_s is particle mass, and p_s is the partial pressure. The following species are present: neutral He atoms ($s=n$), electrons ($s=e$), ions ($s=i$), and He atoms in various excited states. The only excited states explicitly considered are the singlet and triplet metastable states ($s=1m$ and $s=3m$). It has been assumed that the number of molecules, doubly charged ions, and negative ions is negligible.

Since the afterglow period is being considered, quasineutrality and zero net current are assumed,

$$n_e = n_i, \tag{1}$$

$$\vec{v}_e = \vec{v}_i. \tag{2}$$

The important atomic processes which are included in the study are the following:

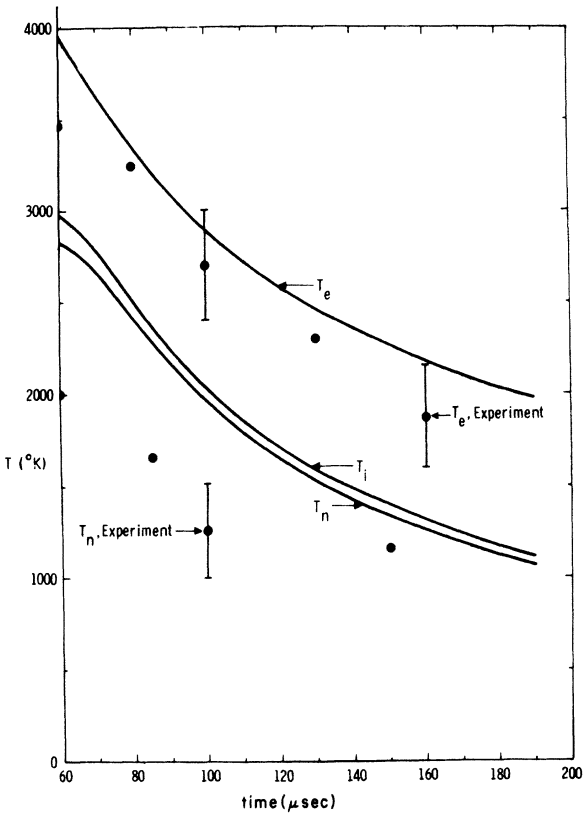

FIG. 2. Temperatures on axis versus time. The solid curves represent the results of the reference run. The data points and error flags illustrate the experimental results.

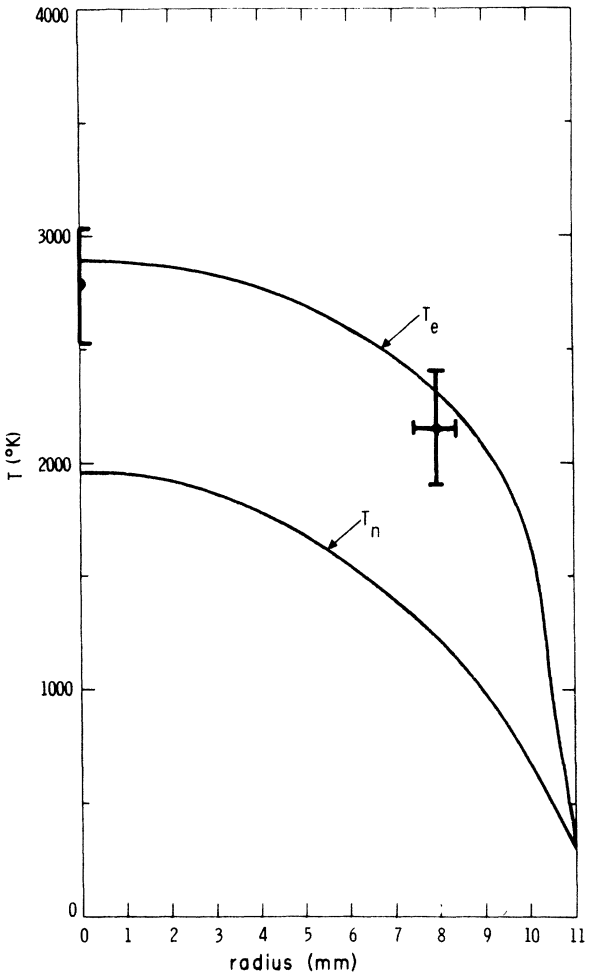

FIG. 3. Electron and neutral gas temperature profiles at 100 μsec. The solid curves represent the results of the reference run. The data points and error flags illustrate the experimental results.

$$He^+ + e + e \xrightarrow{\alpha} He^* + e \ , \tag{3}$$

$$He(2^3S) + e \xrightarrow{\eta} He(1^1S) + e \ , \tag{4}$$

$$He(2^3S) + He(2^3S) \xrightarrow{\beta} He(1^1S) + He^+ + e \ , \tag{5}$$

$$He(2^1S) + e \xrightarrow{\chi} He(2^3S) + e \ , \tag{6}$$

$$He^+ + He \xrightarrow{\sigma_{in}} He + He^+ \ , \tag{7}$$

$$e + He \xrightarrow{\sigma_{en}} e + He \ . \tag{8}$$

The various coefficients and cross sections governing the reactions (e.g., recombination, metastable-metastable rate, etc.) are indicated above the arrow and are explicitly discussed in Appendix A. The reaction equivalent to (5) but with either one or two 2^1S metastable helium atoms was not included because in general the population density of 2^1S is expected to be much less than that of 2^3S.

A straightforward conservation law approach was used to formulate the transport equations from Boltzmann's equation. The collision term in each case was evaluated for the average particle. For the electrons (and ions) mass conservation gives, taking processes (3) and (5) into account,

$$\frac{\partial n_e}{\partial t} = -\nabla \cdot n_e \vec{v}_e - \alpha n_e^2 + \beta n_{3m}^2 \ ; \tag{9}$$

for the neutral He atoms,

$$\frac{\partial n_n}{\partial t} = -\nabla \cdot n_n \vec{v}_n + \alpha n_e^2 - \beta n_{3m}^2 \ . \tag{10}$$

A recombination event is considered to have occurred when the recombining electron has reached one of the metastable levels. Though n_n implicitly includes n_{3m} and n_{1m}, separate continuity equations for the metastables are included in order

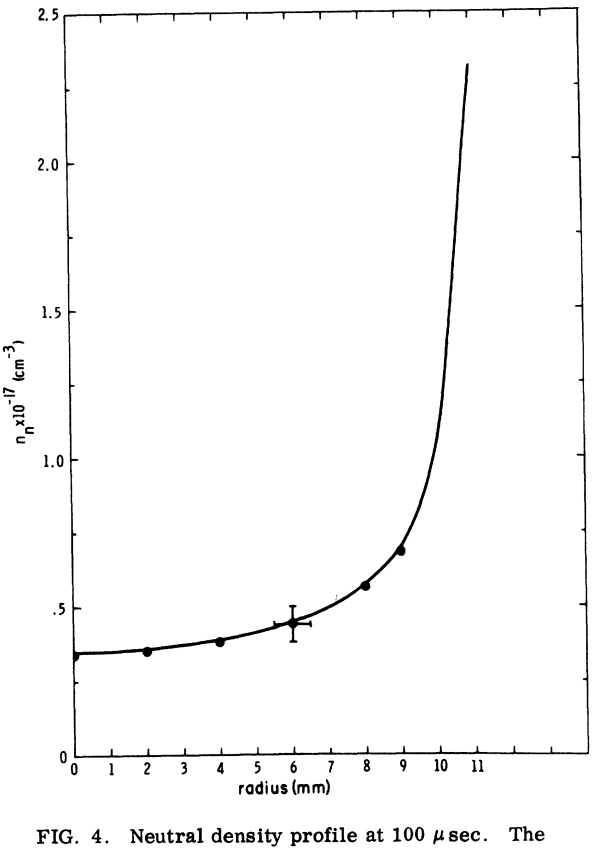

FIG. 4. Neutral density profile at 100 μsec. The solid curve represents the results of the reference run. The data points and error flags illustrate the experimental results.

to calculate n_{3m} and n_{1m} explicitly. These are given by

$$\frac{\partial n_{3m}}{\partial t} = -\nabla\cdot n_{3m}\vec{v}_{3m} + 0.75\alpha n_e^2 - \beta n_{3m}^2 - \eta n_e n_{3m} + \chi n_e n_{1m} \ , \tag{11}$$

$$\frac{\partial n_{1m}}{\partial t} = -\nabla\cdot n_{1m}\vec{v}_{1m} + 0.25\alpha n_e^2 - \chi n_e n_{1m} , \tag{12}$$

where processes (4), (5), and (6) have been taken into account, and it has been assumed that all neutral He atoms resulting from process (3) end up in metastable states in the ratio triplet: singlet = 3: 1. The sensitivity of the results to this latter assumption, and its validity, will be discussed later. In solving Eqs. (11) and (12) it has also been assumed that

$$n_{3m}(\vec{v}_{3m} - \vec{v}_n) = -D_{3m}\nabla n_{3m} \ , \tag{13}$$

$$n_{1m}(\vec{v}_{1m} - \vec{v}_n) = -D_{1m}\nabla n_{1m} \ , \tag{14}$$

where D_{3m} and D_{1m} are the diffusion coefficients for metastables in a background of unexcited He atoms. We take $D_{1m} = D_{3m} = D_M$.

The equations of momentum conservation for the electrons, ions, and neutral atoms are, respectively:

$$\frac{\partial}{\partial t}(m_e n_e \vec{v}_e) = -\nabla\cdot(m_e n_e \vec{v}_e \vec{v}_e) - \nabla P_e - \nabla\cdot\vec{\vec{\pi}}_e + \vec{P}_{ei} + \vec{P}_{en} - e n_e \vec{E} - m_e \vec{v}_e \alpha n_e^2 + m_e \vec{v}_{3m}\beta n_{3m}^2 \ , \tag{15}$$

$$\frac{\partial}{\partial t}(m_i n_e \vec{v}_e) = -\nabla\cdot(m_i n_e \vec{v}_e \vec{v}_e) - \nabla P_i - \nabla\cdot\vec{\vec{\pi}}_i + \vec{P}_{ie} + \vec{P}_{in} + e n_e \vec{E} - m_i \vec{v}_e \alpha n_e^2 + m_i \vec{v}_{3m}\beta n_{3m}^2 \ , \tag{16}$$

$$\frac{\partial}{\partial t}(m_n n_n \vec{v}_n) = -\nabla\cdot(m_n n_n \vec{v}_n \vec{v}_n) - \nabla P_n - \nabla\cdot\vec{\vec{\pi}}_n + \vec{P}_{ne} + \vec{P}_{ni} + m_n \vec{v}_e \alpha n_e^2 - m_n \vec{v}_{3m}\beta n_{3m}^2 \ . \tag{17}$$

The $P_{s_1 s_2}$ are the rates at which momentum is transferred from species 2 to 1 in all collisions for which no new species are produced. Expressions for the $\vec{P}_{s_1 s_2}$ in terms of basic reaction rates are given in Appendix A. The quantity $p_s = n_s k T_s$ is pressure, $\vec{\vec{\pi}}_s$ is the nondiagonal part of the pressure tensor, and $\vec{E}$ is the space charge electric field which causes the ambipolar motion implied by Eq. (2). The βn_{3m}^2 terms in these equations are included in order to account for momentum transfer by event (5).

In solving the system of equations, Eqs. (15), (16), and (17) are replaced by the sum (15) and (16) and the sum of (15), (16), and (17). This eliminates the electric field and the $\vec{P}_{ei} = -\vec{P}_{ie}$ terms. We also set $m_i = m_n$ and $-\nabla\cdot\vec{\vec{\pi}}_s = \nu\vec{v}_s$. The term $-\nabla\cdot\vec{\vec{\pi}}_s$ is usually approximated by a viscosity coefficient times

$$[\nabla^2\vec{v}_s + \tfrac{1}{3}\nabla(\nabla\cdot\vec{v}_s)] \ .$$

Thus ν is a viscosity coefficient (whose value is obtained from ordinary kinetic theory) divided by the square of a characteristic length. This approximation is justified by the independence of the solution on the value used for ν, as will be discussed later.

The equations of energy conservation for electrons, ions, and neutrals are, respectively,

$$\frac{\partial}{\partial t}(\tfrac{3}{2}p_e) = \nabla\cdot(K_e\nabla T_e) - \tfrac{5}{2}\nabla\cdot(p_e\vec{v}_e) + kT_e\alpha n_e^2[\ln(I/kT_e) - \tfrac{1}{2}] + R_{ei} + R_{en} + \beta' n_{3m}^2 + \eta' n_e n_{3m} + \gamma\chi n_e n_{1m} \ , \tag{18}$$

$$\frac{\partial}{\partial t}(\tfrac{3}{2}p_i) = \nabla\cdot(K_i\nabla T_i) - \tfrac{5}{2}\nabla\cdot(p_i\vec{v}_e) - \tfrac{3}{2}kT_i\alpha n_e^2 + R_{ie} + R_{in} + \tfrac{1}{3}\beta' n_{3m}^2 \quad , \tag{19}$$

$$\frac{\partial}{\partial t}(\tfrac{3}{2}p_n) = \nabla\cdot(K_n\nabla T_n) - \tfrac{5}{2}\nabla\cdot(p_n\vec{v}_n) + \tfrac{3}{2}kT_i\alpha n_e^2 + R_{ne} + R_{ni} + \tfrac{1}{3}\beta' n_{3m}^2 \quad . \tag{20}$$

The $R_{s_1s_2}$ are the rates at which energy is transferred from species 2 to 1 in all collisions for which no new species is produced. Expressions for the $R_{s_1s_2}$ in terms of basic rates are explicitly given in Appendix A. These energy equations equate the rate of change of a species' internal energy

$$\frac{\partial}{\partial t}(\tfrac{3}{2}n_s kT_s)$$

in a volume element to the rate at which heat is conducted into the volume $\nabla\cdot(K_s\nabla T_s)$, plus the rate at which internal energy is convected into the volume $-\tfrac{3}{2}\nabla\cdot(p_s\vec{v}_s)$, plus the rate at which pressure work is done on the volume $-\nabla\cdot(p_s\vec{v}_s)$, plus the rate of energy transfer to the species by all types of collisions. The explicit expressions for the thermal conductivities K_s are given in Appendix A. The third term on the right-hand side of (18), where I is the ionization potential of He, is the net rate of heating of the electrons due to recombination.[4] The $\beta' n_{3m}^2$ terms in (18), (19), and (20), represent the heating due to the reaction given by Eq. 5. The average energies of the products of the reaction are 3 eV per heavy particle and 9 eV for the electron.[5] Thus, the coefficient β' is given by

$$\beta' = 9 \text{ eV} \times \beta. \tag{21}$$

The quantity η' is given by

$$\eta' = 19.83 \text{ eV} \times \eta \quad , \tag{22}$$

since the triplet metastable state is 19.83 eV above the ground state. The term $\gamma\chi n_e n_{1m}$ in Eq. (18) is the electron heating due to process (6), where

$$\gamma = 0.8 \text{ eV} \tag{23}$$

is the energy separation of the singlet and triplet metastable states.

The energy equations neglect the work done by $\vec{E}$ on the charged species and the energy of mass motion.[6] Estimates justify the former, and the latter corresponds to assuming $m_s v_s^2 \ll kT_s$, or that flow speeds are small compared to sound speeds. Calculations show this to be an excellent assumption.

Several comments should be made about the system of equations. The temperatures T_s and pressures p_s are defined in terms of $\vec{v}_s$ rather than in terms of the center-of-mass velocity of the entire plasma. This distinction is negligible since it amounts once again to neglecting v_s compared to $(kT_s/m_s)^{1/2}$.[7] Note that the possibility has been allowed that all three temperatures (T_e, T_i, and T_n) are different despite the fact that collision times ($\tau_{in} < 10^{-7}$ sec and $\tau_{ei} < 10^{-6}$ sec) are much shorter than the duration of the observation ($\sim 10^{-4}$ sec). Diffusion coefficients have not been used in Eqs. (9) and (10) because, for this problem, with its nonuniform, hot neutral gas, $n_e\vec{v}_e = -D_a\nabla n_e$ is unjustified (*a priori*). A discussion of this "diffusion approximation" is given in Appendix B. The lengthier but more general route of including the momentum conservation equations (15), (16), and (17) was taken. The use of diffusion coefficients in Eqs. (13) and (14) for the metastables is also only approximate, but it will later be seen that this leads to negligible error.

The many parameters needed to solve the set of equations are available in the literature although some are known only to within a factor of 2. These are fully discussed in Appendix A. A main assumption in the solution is that the nonequilibrium problem is sufficiently close to equilibrium to justify the assumption of nearly Maxwellian distribution functions.

B. Method of Solution

In the application of the equations given in the previous section to the problem of an afterglow plasma in a long cylindrical tube, it was assumed that the wall remains at nearly room temperature throughout the time of observation. The justification for this assumption is that a calculation showed that the wall has a sufficiently large heat capacity to absorb the plasma energy with no appreciable temperature rise and a large enough thermal conductivity so that the heat absorbed does not remain near the inside surface of the glass. In light of the above discussion, together with the known efficiency of energy transfer from atoms to walls,[8] it was assumed that the neutral helium next to the wall is in equilibrium with the wall at the wall temperature of 300°K. In addition, since the neutral atom density is very high near the wall, $\sim 10^{18}$ cm^{-3}, the electron-neutral equilibration time is small and the additional assumption was made that $T_e = 300$°K at the wall. The latter condition can be relaxed as it has little effect on the solution as long as T_e is sufficiently cooler at the wall than it is in the center of the tube, a condition which is surely satisfied. The boundary condition imposed on the average velocity of the species $\vec{v}_s$ is that each be zero at the wall. This neglects surface neutralization of electrons and ions, but should not lead to significant error because the free electrons recombine very rapidly as they approach the wall (due to the strong inverse temperature dependence of α) and only a small percentage of the total will reach the

wall. Plasma sheath effects have been neglected.

Both axial and azimuthal symmetry were assumed. The former is justified by the large ratio of tube length to diameter. Thus, the independent variables are time t and the radial coordinate r. The velocities $\vec{v}_s$ have only radial components. These conditions and the appropriate rates were incorporated into the equations, and the three momentum equations were combined into two as discussed in the previous section. The result was a system of nine partial differential equations in the nine unknowns n_e, n_n, n_{3m}, n_{1m}, T_e, T_i, T_n, $\vec{v}_e$, and $\vec{v}_n$. The equations are coupled and nonlinear, but they are first order in t. Using a straightforward differencing method, a computer program was written which takes initial profiles [$n_e(r)$, $n_n(r)$, etc.] of the nine quantities and carries them forward in time.

The details of the program are not discussed here. The results were checked inasmuch as the solutions are independent of mesh size (Δr) and the size of the time step (Δt). As an additional check the program periodically calculates the total number of neutral atoms and electrons in the tube; the sum must remain constant.

C. Reference Run and Initial Conditions

Numerical solutions are often strongly dependent on the assumed initial conditions. Fortunately, in the problem solved here the dependence on initial conditions is slight after about 10 μsec. This permitted the use of initial conditions which were known to be inaccurate and consequently gave assurance that the numerical solutions were not dictated by the chosen initial conditions. The electron density and electron temperature profiles were permitted to evolve from initially assumed "uniform" distributions and the metastable density was allowed to evolve from an initially zero value. The particular initial profiles which were used in this study are shown in Fig. 5 and initial $n_{3m}(r)$, $n_{1m}(r)$, $v_e(r)$, and $v_n(r)$ were set equal to zero. The initial $n_e(r=0)$, $T_e(r=0)$, and $T_n(r=0)$ were chosen to agree with the experimental values at 50 μsec after the initiation of the discharge. At earlier times in the afterglow the experimental plasma was not sufficiently symmetric. The initial n_n profile was chosen to agree with experiment out to $r=8$, the limit of trustworthy measurements. The n_n values beyond $r=8$ were picked somewhat arbitrarily, but with the requirement that the total number of particles in the tube be equal to the value prior to the discharge. The n_e and T_e profiles were taken to be flat except near the wall, where the values were chosen arbitrarily (except that $T_e = 300°K$ at $r=11$). The T_n profile was selected to make the pressure uniform across the tube. When this condition was not imposed pressure gradients disappeared in a time equal to the time required for a sound wave to traverse a distance of a few tube diameters; for the plasma considered here this is a few tens of microseconds. The assumption that $T_i = T_n$ initially is based on the good thermal contact between the heavy particles. This assumption turns out to be only approximately correct.

The mean free path of the ~ 20 eV electron re-

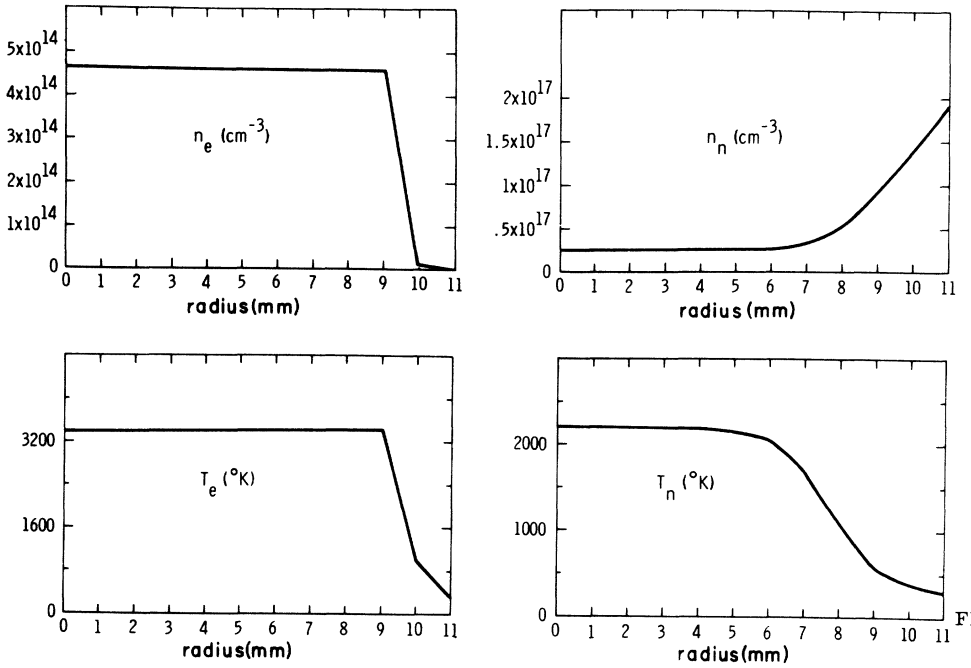

FIG. 5. Initial conditions for reference run.

sulting from process (4) is about the same as the tube radius.[9] Thus it is estimated that about half the kinetic energy of the 20 eV electrons resulting from this reaction will be dissipated in the wall rather than in the background gas. In the reference run Eq. (22) was replaced by $\eta' = 10\ \text{eV}\cdot\eta$, as a best approximation. (This change was unimportant in the final results.) The mean free path of the 9 eV electron from process (5) is much less than the tube radius and direct wall loss is assumed negligible.

The results of the reference run are given in Fig. 1–4 and 6–8. The initial conditions were found to grossly affect the solution during the time 50–60 μsec, but after this time the solution is very nearly independent of the initial values, as discussed below. For this reason the results are not presented for $t < 60$ μsec, as they may be misleading.

The time decay of n_e in the tube center is shown in Fig. 1 together with some experimental points and their error bars. The value of the three terms on the right-hand side of Eq. (9) are shown in Fig. 6. The $\beta n_{3m}{}^2$ term is a source of free electrons and the other terms are loss terms. Note that while recombination is the most important term, neither the motion of the electron gas nor metastable-metastable collisions can be neglected in the electron particle conservation equation.

Figure 2 shows the decay of the temperatures, and some experimental points for T_e and T_n. Note that T_i remains slightly higher than T_n while the electrons stay much hotter than the heavy particles. The electron temperature is maintained above T_i and T_n by processes (3), (4), (5), and (6). The rate of energy transfer by each of these processes is illustrated in Fig. 7. The rate of transfer of thermal energy from the electrons to the ions R_{ei} is shown on the same graph for comparison.

The neutral atom density spatial profile at $t = 100$ μsec is illustrated in Fig. 4 together with some experimental points. The corresponding T_n spatial profile is nearly the inverse of the $n_n(r)$ spatial profile giving a nearly uniform total pressure ($p_{\text{tot}} = n_n k T_n$ + small correction for ions and electrons). There is a slight pressure gradient (at 100 μsec the pressure at the wall exceeds that in the center by about 1%) and it is this gradient that determines the bulk motion of the gas. The average velocity of the neutrals $\vec{v}_n$ and the charged particles $\vec{v}_e$ are shown in Fig. 8 for $t = 100$ μsec. The charged particles are moving towards the wall ($+\vec{v}_e$) as is to be expected since both n_e and T_e are lower at the wall than in the center, while the neutrals are moving inwards ($-\vec{v}_n$) because of the slight pressure gradient.

The present section is concluded by explicitly discussing the sensitivity of our results to

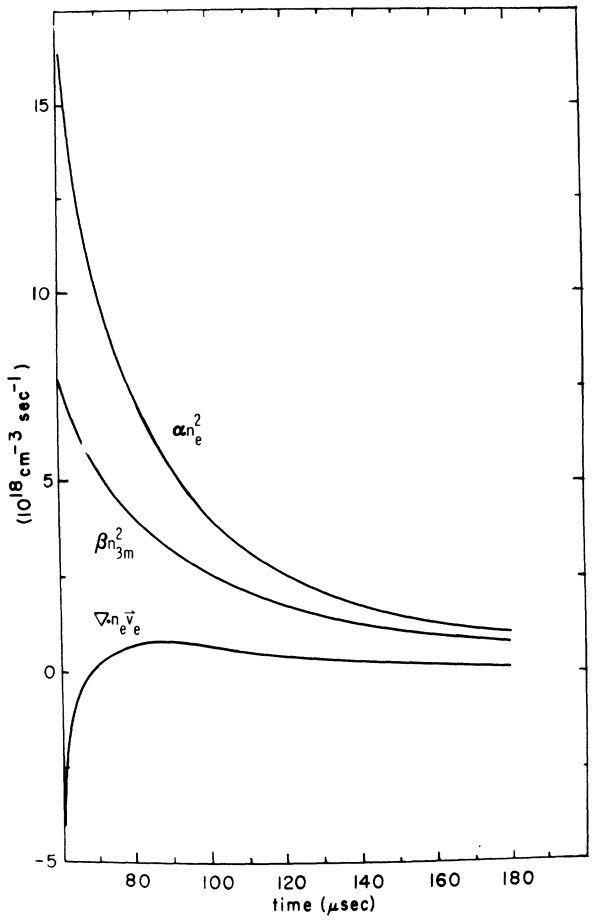

FIG. 6. Reference Run: $\alpha n_e{}^2$, $\nabla\cdot n_e\vec{v}_e$ and $\beta n_{3m}{}^2$ on axis versus time. The negative portion of the $\nabla\cdot n_e\vec{v}_e$ curve at early time is caused by the interaction of the free electrons with the inwardly flowing neutral gas.

changes in the chosen initial conditions. In obtaining Table I, each computer run was identical with the reference run except for the change in the particular initial condition listed; e.g., the first listed run was simply the reference run except instead of starting with zero initial velocities the assumed initial velocities were $\vec{v}_e = 10^3$, $\vec{v}_n = -2 \times 10^3$ for all r (except of course at $r = 0$ and the wall where $\vec{v}_e$ and $\vec{v}_n$ are always zero). Table I only shows the differences at 60 μsec; generally the differences become less at later times, and in no case did the difference become substantially more.

The first three runs in Table I illustrate that the results are independent (within reasonable limits) of initial velocity, ion temperature, and the values of n_e near the wall. In the latter run n_e was assumed to be uniform out to $r = 10$ mm (see Fig. 5). The fourth run shows that the results have only a

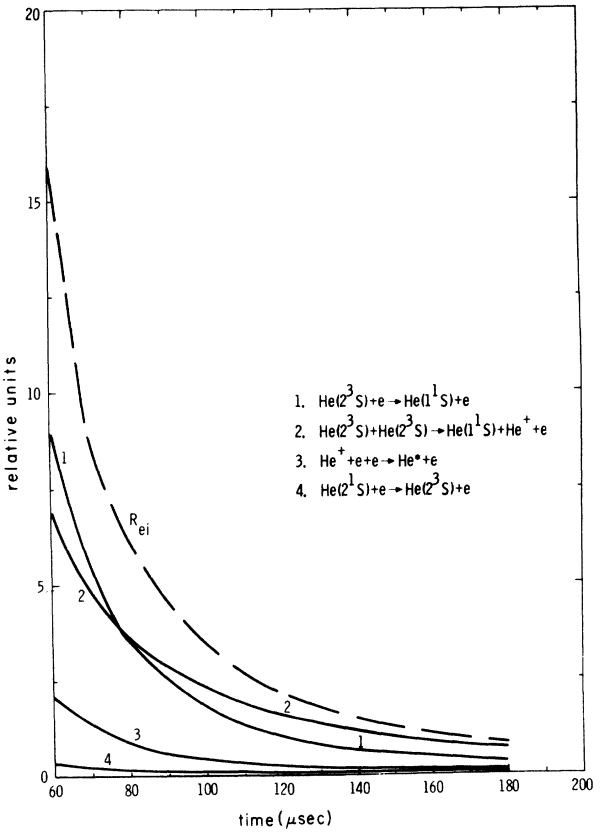

FIG. 7. Reference Run: Electron heating rates evaluated on axis versus time.

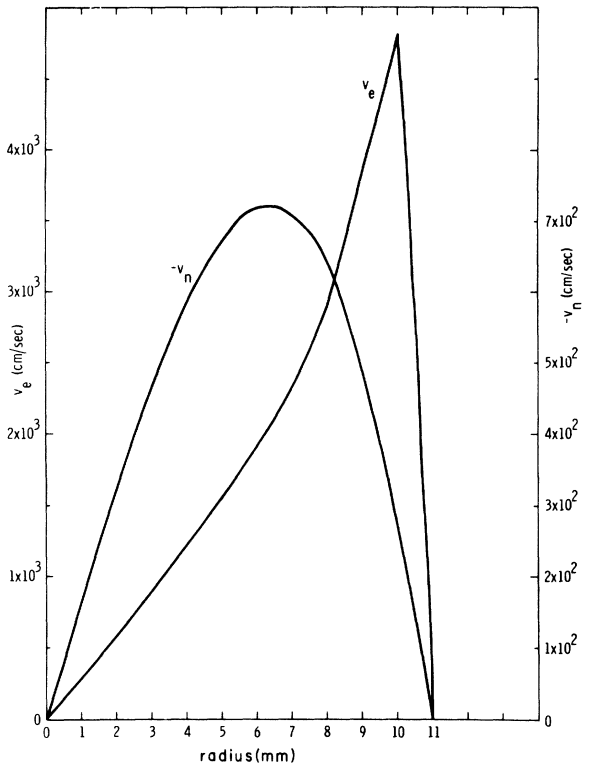

FIG. 8. Reference Run: v_e and v_n profiles at 100 μ sec.

slight dependence on the initial metastable density; the dependence of n_{3m} on its initial value is shown in Fig. 9. It is very important that the solution is not susceptible to variations of the initial value of n_{3m} because this quantity was not measured. Since the solution is not sensitive to n_{3m}, it also follows that it is not strongly dependent on its assumed initial spatial profile. Runs 5 and 6 show the effect of starting with quadratic, rather than flat, n_e and T_e profiles (keeping the values in the center the same). The particular quadratic profiles chosen were a good fit to the experimental profiles.[2] The solution is seen to be independent of the assumed initial T_e profile, but somewhat dependent on the initial n_e profile. The spatial behavior of n_e for initially flat and quadratic n_e profiles is shown in Fig. 10 for various times. The profiles were normalized at $R = 0$ for purposes of comparison and are found to be quite similar after 10 μsec. The relative magnitudes of the electron source and sink terms in the electron conservation equation, Eq. (9), for the initially quadratic profile are plotted in Fig. 11. This is to be compared with the corresponding results for an initially flat n_e profile, Fig. 6. The results are essentially the same for each case.

Runs 7–10 in Table I illustrate the dependence of the solution on variations in the initial values of measured parameters. In each case the quantity has been lowered by the amount of its experimental uncertainty. In run 7, the center value of T_n was lowered by 400°K, T_n elsewhere being changed to keep the pressure constant across the tube. (Although starting with a slightly nonuniform pressure does not affect the results.) In runs 9 and 10 values of n_e and T_e were decreased by the indicated values for $0 \leq r \leq 9$ mm.

In summary, a reference solution has been obtained and it was found that this solution is consistent with experiment and insensitive to reasonable variations (i.e., those we think physically possible) in the unknown initial conditions. In the next section a study is made of the importance of the various processes in the plasma decay by varying rate coefficients, cross sections, etc. around the values used in the reference run. Thus, although all solutions obtained in the next section are for a particular set of initial conditions (those used in the reference run) it is reasonable to assume that the results obtained do indeed apply to the actual experimental plasma. In fact, it is our contention that these results apply at least semiquantitatively to any afterglow helium plasma with densities, temperatures, and geometry comparable to the one

TABLE I. Dependence of plasma densities and temperatures on initial conditions.

Variation in initial condition	% difference in values at tube center at 60 μsec			
	n_e	T_e	T_n	n_n
(1) v_e: $0 \rightarrow 10^3$ cm/sec				
v_n: $0 \rightarrow -2\times10^3$ cm/sec	0.3	0.0	0.1	0.2
(2) T_i (center): 2200 → 2982° K	0.2	0.1	0.2	0.2
(3) $n_e(r=10)$: $10^{13} \rightarrow 4.6\times10^{14}$ cm^{-3}	0.2	0.7	1.9	1.3
(4) n_{3m}: $0 \rightarrow 3.7\times10^{13}$ cm^{-3}				
n_{1m}: $0 \rightarrow 1.7\times10^{12}$ cm^{-3}	5.3	2.2	3.5	0.3
(5) T_e: flat → quadratic	0.1	0.0	0.0	0.0
(6) n_e: flat → quadratic	14.0	6.1	9.7	5.0
(7) T_n (center): 2200 → 1800° K	4.4	3.0	7.6	3.2
(8) n_n(everywhere) decreased by 10%	0.5	0.3	0.5	9.0
(9) n_e $0 \le r \le 9$: decreased by 6.5%	4.8	1.8	2.8	0.2
(10) T_e $(0 \le r \le 9)$: 3400 → 2900° K	0.2	0.1	0.1	0.0

studied here. The effect of the latter is discussed in Appendix C.

IV. VARIATION OF PARAMETERS

The parameters are grouped into three classes: those which have almost no effect on the solution (Class I), those which have a small effect (Class II), and those which have a large effect (Class III).

Table II illustrates the change in the solution at

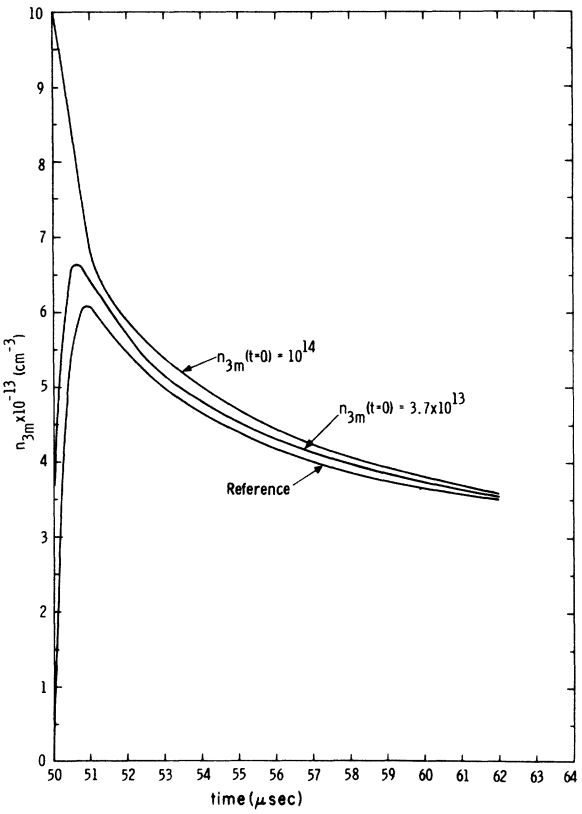

FIG. 9. n_{3m} on axis versus t, showing effect of starting with nonzero initial n_{3m} and n_{1m}.

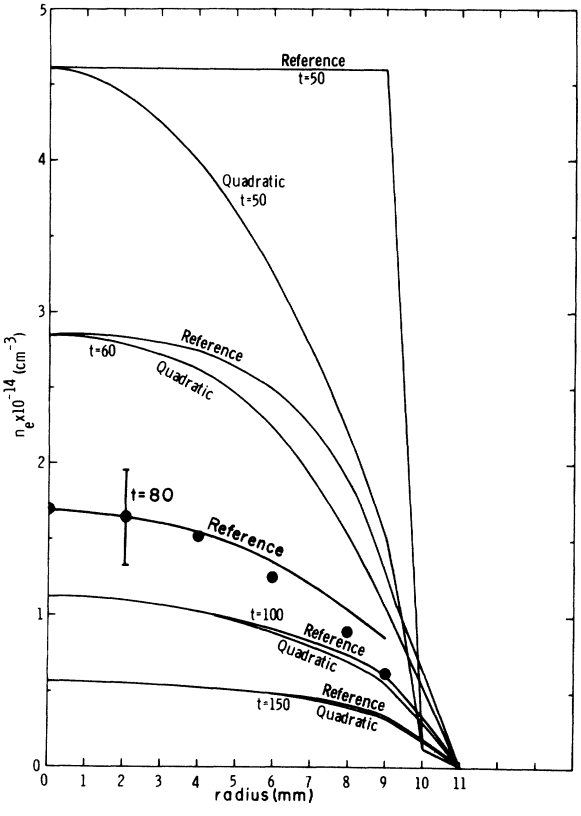

FIG. 10. Dependence of n_e profile on initial n_e profile. The profiles are normalized at $r=0$ for purposes of comparison. The data points and error flags illustrate the experimental results at $t=80$ μsec.

TABLE II. Variation of plasma densities and temperatures when Class I parameters are decreased by 50%.

Parameter	% variation in values at tube center at 60 and 80 μsec							
	n_e		T_e		T_n		n_n	
	60	80	60	80	60	80	60	80
σ_{en}(Eq. 8′)	0.2	0.5	0.3	0.4	0.4	0.4	0.1	0.0
K_i(Eq. 26)	0.0	0.0	0.0	0.0	0.0	0.0	0.0	0.0
χ (Eq. 6′)	0.0	0.0	0.0	0.0	0.0	0.0	0.0	0.0
D_M(Eq. 24)	0.2	0.1	0.1	0.0	0.0	0.0	0.1	0.1
ν (viscosity)	2.9	0.3	0.4	0.0	0.6	0.2	4.5	0.5

60 and 80 μsec caused by decreasing Class I parameters by a factor two. A value 0.0 means the change was less than 0.05%.

The percent changes in the solutions caused by decreasing Class II parameters by a factor two are given in Table III, where we have indicated whether the perturbed result was above (+) or below (−) that of the reference.

As discussed above, the reference run actually used $\frac{1}{2}\eta'$, so in the third run of Table III heating of the electron gas by process (4) was decreased from 10 eV to 5 eV per event. Since we have modified η' rather crudely to approximate the loss of 20 eV electrons to the wall, it is important that the solution is not very sensitive to η' variations.

Table IV illustrates how Class III parameters affect the solution when each is decreased by a factor of two. In the last run shown, the assumption that all neutral atoms formed by recombinations end up in metastable states has been changed to the assumption that only half of them do, i.e., 0.75 and 0.25 in Eqs. (11) and (12) have been changed to 0.375 and 0.125. The resulting large variation is interesting but only academic, since the plasma of interest is optically thick for reso-

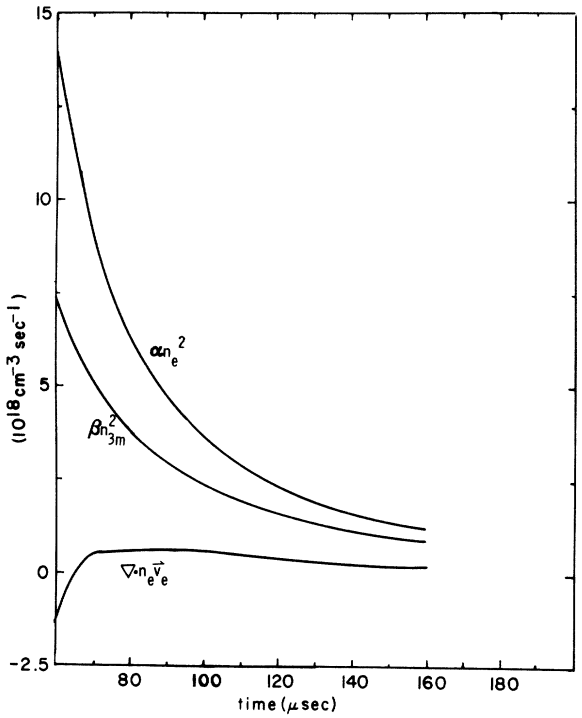

FIG. 11. αn_e^2, $\nabla \cdot n_e \vec{v}_e$, and βn_{3m}^2 on axis versus time for initially quadratic n_e profile. The negative portion of the $\nabla \cdot n_e \vec{v}_e$ curve at early time is caused by the interaction of the free electrons with inwardly flowing neutral gas.

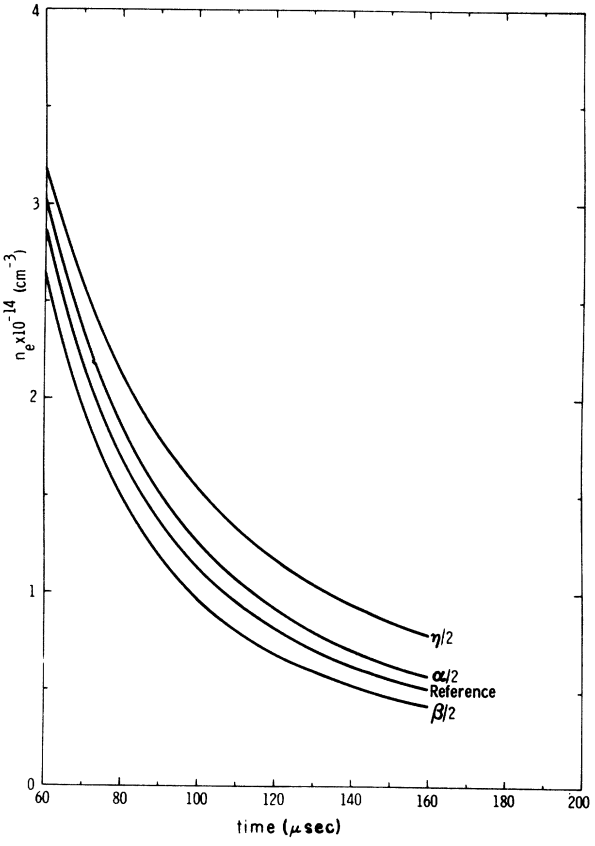

FIG. 12. Effect of separately decreasing α, β, and η by a factor two on electron density decay in tube center.

TABLE III. Variation of plasma densities and temperatures when Class II parameters are decreased by 50%.

Parameter	% variation in values at tube center at 60 and 80 μsec.							
	n_e		T_e		T_n		n_n	
	60	80	60	80	60	80	60	80
K_e(Eq. 25)	+0.7	+1.4	+1.2	+1.9	+0.2	+0.5	−0.1	−0.2
Recombination Heating Term (See Eq. 18)	−0.9	−1.1	−1.1	−1.1	−0.3	−0.4	+0.2	+0.2
η' (Eq. 22)	−3.0	−4.0	−4.4	−4.3	−1.0	−1.3	+0.6	+0.6

nance radiation. Thus, excited He atoms can decay to the ground state only via superelastic collisions with electrons, and it follows that most excited atoms will decay to the metastable level. Thus the coefficients in Eqs. (11) and (12) will necessarily be close to 0.75 and 0.25.

The time behavior of n_e, T_e, and T_n in the tube center for the first three runs in the Class III table is compared in Figs. 12 and 13 with the reference solution. The solution is seen to be more sensitive to η than to either α or β. When η is decreased, triplet metastables are not destroyed as rapidly by process (4). The corresponding increase in n_{3m} and decrease in η roughly compensate each other in terms like $\eta m_e n_{3m}$ in Eq. (11) and $\eta' n_e n_{3m}$ in Eq. (18). However, the heating due to process (5), since it is proportional to n_{3m}^2, is considerably increased and consequently causes higher temperatures to be maintained. Because of the $T_e^{-9/2}$ in Eq. (3′), a higher value of T_e decreases the rate of recombination and a higher n_e results. This explanation is of course only qualitative. It is a basic property of this problem that there are many important processes which are strongly coupled and often compensatory. It is difficult to separate cause and effect and indeed difficult to predict *a priori* what the qualitative effect of changing a parameter will be.

The time behaviors of n_e, T_e, and T_n in the tube center which result with factor of $\frac{1}{2}$ changes in σ_{in} and τ_{ie} are shown in Figs. 14 and 15. To show the importance of K_n, we have included in these figures the solution obtained when the neutral thermal conductivity, Eq. (27), is replaced by $K_n = 336 T_n^{0.75}$. Note that such a change brings the theoretical values of T_n into closer agreement with the experimental values. However, Eq. (27) is known to be quite accurate, and the discrepancy between theoretical and experimental T_n probably results from some other cause such as wall effects or impurities. Runs with variations in β' or 0.75 and 0.25 have not been plotted since the latter have been considered as known quantities and β' is related to β by a constant.

Thus far the discussion has been concerned with variations by a factor of two in rate coefficients and cross sections. It is important to consider more realistic uncertainties in the parameters. It is unlikely that the actual uncertainty in any of the Class I or II parameters is great enough to shift it to Class III. The Class III parameters can be divided into two groups: those which are more accurate than a factor of two (K_n, σ_{in}, η, and 0.75 and 0.25), and those which may be uncertain by a factor two [τ_{ei}, α, and β (and hence β')].

The coefficient η depends on the cross section $\sigma(2^3S \rightarrow 1^1S)$ which can be obtained exactly from $\sigma(1^1S \rightarrow 2^3S)$ by detailed balancing. The inaccuracy in the latter cross section[10] is expected to be con-

TABLE IV. Variation of plasma densities and temperatures when Class III parameters are decreased by 50%.

Parameter	% variation in values at tube center at 60 and 80 μsec							
	n_e		T_e		T_n		n_n	
	60	80	60	80	60	80	60	80
β (Eq. 5′)	−7.7	−12.2	−2.3	−4.0	−4.1	−5.9	+0.2	+1.4
α (Eq. 3′)	+5.9	+9.5	−9.0	−7.9	−2.5	−1.5	+1.1	+0.6
η (Eq. 4′)	+10.1	+21.0	+3.2	+7.5	+3.7	+9.8	−2.8	−3.1
σ_{in}(Eq. 7′)	−5.2	−16.5	−0.7	−4.1	−3.3	−5.4	+0.6	+3.1
K_n(Eq. 27)	−2.8	−2.8	+2.8	+6.3	+6.8	+19.1	−4.8	−12.8
τ_{ei}(Eq. 28)	−4.6	−6.8	−4.6	−5.5	+7.6	+6.3	+0.7	−0.4
β' (Eq. 21)	−4.9	−6.4	−5.9	−7.3	−4.7	−5.9	+0.6	+1.5
0.75, 0.25 (Eqs. 11 and 12)	−29.8	−45.9	−17.4	−24.3	−13.4	−20.6	+1.8	+5.3

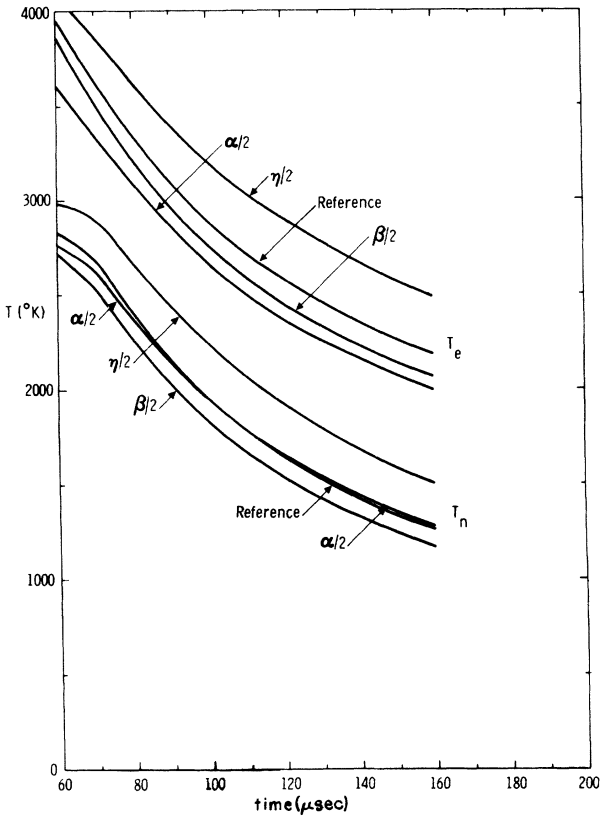

FIG. 13. Effect of separately decreasing α, β, and η by a factor two on temperature decay in tube center.

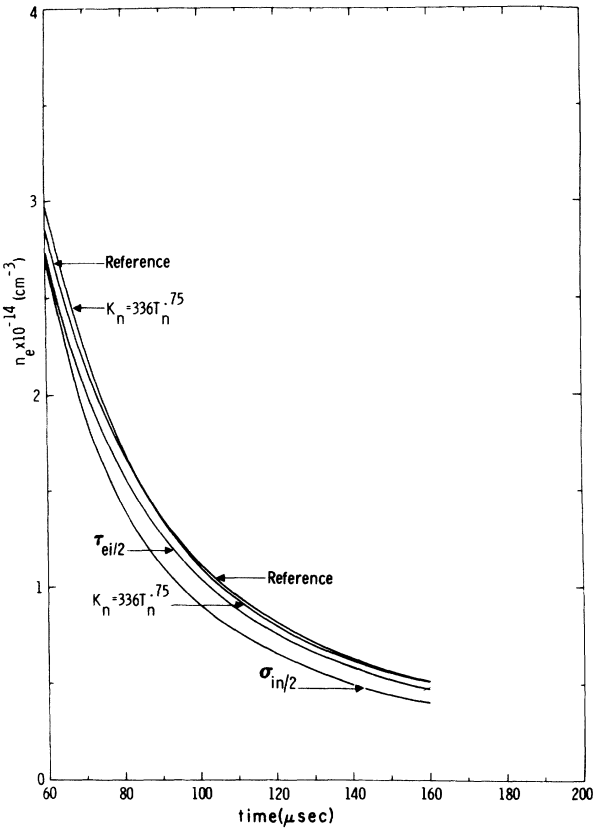

FIG. 14. Effect of separately varying τ_{ie}, σ_{in}, and K_n on electron density decay in tube center.

siderably less than a factor of two. Consequently, η should be more accurate than a factor of two, even with the piecewise linear approximation to σ given in Appendix A.

Concerning the accuracy of τ_{ei} and α, one can say that the results of experimental investigations indicate that the theoretical values used are consistent with experimental results. A study of past experiments designed to determine α in helium indicates that the experimental determination of this coefficient is probably no better than a factor of two (in the range of parameters considered here). The metastable-metastable rate β is probably the most inaccurate parameter in this paper, and this rate grossly affects the net decay rate of the free electrons. It is obvious from Fig. 6 that even in the absence of the convection term $\nabla \cdot n_e \vec{v}_e$, it would be rather presumptious to infer a recombination coefficient α from electron density decay curves without consideration of metastables. For example, at 80 μsec, the net decay rate of n_e is approximately only half as large as αn_e^2. Furthermore, it is clear from Fig. 12 that the metastable-metastable rate coefficient β must be known more accurately than a factor two, in order to obtain an accurate experimental determination of the recombination coefficient from experimental n_e decay curves.

V. CONCLUSIONS

In this paper solutions have been obtained for a complex but realistic set of three-temperature transport equations which have been found adequate to describe the behavior of a laboratory helium afterglow plasma. We have used the best value in the literature for each parameter, and have studied the sensitivity of solutions to uncertainties in these parameters. From this study the six most important parameters in determining the plasma behavior are found to be α(three-body recombination), β(metastable-metastable collisions), η(electron-metastable super-elastic collisions), τ_{ei}(time of energy equipartition between electrons and ions), σ_{in}(charge-transfer), and K_n(neutral gas thermal conductivity).

It has been shown that the electron temperature is maintained above the temperatures of the neutral atoms and ions by atomic processes which supply kinetic energy to the electron gas. The primary atomic processes which heat the electrons are

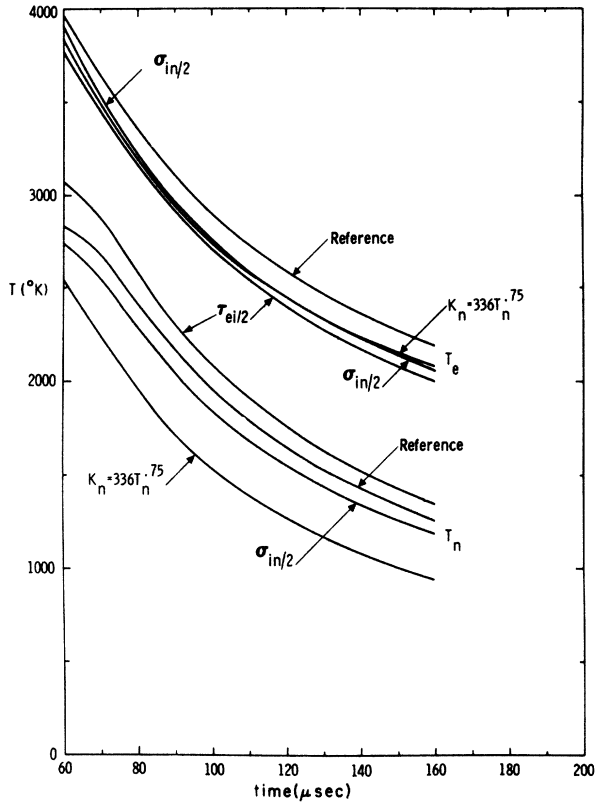

FIG. 15. Effect of separately varying τ_{ie}, σ_{in}, and K_n on temperature decay in tube center.

superelastic collisions of electrons with metastable atoms and metastable-metastable collisions. These sources of thermal energy are also of major importance in the cause and maintenance of spatial gradients in T_e, T_i, and T_n.

Free electrons are lost from the volume mainly by recombination as is shown in Fig. 6. However, the decay of n_e is primarily determined by the relaxation of T_e. This dependence on T_e arises because of the temperature dependence of the recombination coefficient. Thus while the electrons are lost from the volume mainly by recombination, the decay of n_e is principally determined by the thermal conductivity of the background gas, the diameter of the container, and energy equilibration times.

The results indicate that an accurate experimental determination of the recombination coefficient in a helium plasma, similar to the one studied in this work, is difficult and at present probably not more accurate than a factor of two. This error is due primarily to the uncertainty in assessing the effect of the metastable-metastable collision term in the electron mass conservation equation.

The results presented strictly apply only for the given diameter tube and initial conditions. However, as the discussion of Sec. IV indicates, the Class III parameters (Table IV) can be expected to remain the dominant coefficients over a range of plasma conditions. The discussion of Appendix C indicates that Class III parameters remain dominant with variation of the tube diameter by a factor of four (even though their relative importance varies). The results of Sec. IV and Appendix C indicate that the results of this work are qualitatively pertinent to a range of helium afterglow plasmas centered about the plasma considered in this paper.

ACKNOWLEDGMENT

The authors wish to thank J. R. Banister for many helpful discussions.

APPENDIX A: THE RATE AND TRANSPORT COEFFICIENTS

In this appendix we present the explicit forms for the coefficients used in the transport equations. When an equation number is primed, the number itself refers to a process mentioned earlier in the paper. Temperatures are in °K and densities in cm^{-3}.

The recombination coefficient was approximated by

$$\alpha = 1.08\times10^{-8} n_e T_e^{-9/2} \text{ cm}^3 \text{ sec}^{-1} \quad . \tag{3'}$$

This three-body recombination coefficient[11,12] is expected to be quite good in the range of plasma parameters considered.

The cross section for the electron superelastic collision $2^3S - 1^1S$ was obtained from Morrison and Rudge.[10] In particular they give $1^1S - 2^3S$. Using detailed balance one obtains the inverse reaction. We then represent the latter cross section by a piecewise linear approximation (in units of $10^{-2}\pi a_0^2$),

$$\sigma = 968E + 14.4 \quad (E \leq 0.022) \ ,$$

$$\sigma = -170E + 39.5 \quad (E \leq 0.022) \ ,$$

where E is electron energy in eV. The appropriate integration is then made over a Maxwellian distribution to give

$$\eta = 1.34\times10^{-11} T_e^{1/2} \text{ cm}^3 \text{ sec}^{-1} \quad . \tag{4'}$$

We used the cross section of Phelps and Molnar[13] for the metastable-metastable collision. While their value was for 300°K we have assumed no temperature dependence for the calculation.

$$\sigma_{mm} = 10^{-14} \text{ cm}^2 \ ,$$

$$\beta = 1.04\times10^{-10} T_n^{1/2} \text{ cm}^3 \text{ sec}^{-1} \quad . \tag{5'}$$

The cross section for singlet-triplet metastable conversion was obtained from Marriott.[14] The theoretical cross section is a factor of two lower than

TABLE V. Effect of varying tube radius.

Radius	Values at $t = 100$ μsec n_e (cm^{-3})	T_e (° K)	T_n (° K)	n_n (cm^{-3})
2.2 cm	1.52×10^{14}	3846	3340	2.51×10^{16}
1.1 cm	1.12×10^{14}	2892	1959	3.51×10^{16}
0.55 cm	0.60×10^{14}	1419	862	4.72×10^{16}

that of Phelps at 0.026 eV.[15] Consequently, in an attempt to correlate the experiment and theory, Marriott's cross section has been multiplied by a factor of two. In particular we represented the theoretical cross section, in the region of interest, by $312\pi a_0^2 \exp(-1.75E)$ where E is electron energy in eV. The rate χ was obtained by the appropriate integration over a Maxwellian distribution, and includes the effect of inverse collisions:

$$\chi = 6.54\times10^{-9} T_e^{\frac{1}{2}} \times\left(1-\frac{1}{3}\frac{n_{3m}}{n_{1m}} e^{-8060/T_e}\right) \text{cm}^3\,\text{sec}^{-1} \quad . \quad (6')$$

The ion-neutral cross section including both the charge exchange and elastic cross section was estimated by the following:[16]

$$\sigma_{in} = 81\times10^{-16} - 10^{-15}\log_{10}[3k(T_i+T_n)/m_n]^{1/2}\text{cm}^2 \quad . \quad (7')$$

The electron-neutral elastic cross section was obtained from Brown.[17]

$$\sigma_{en} = 5.4\times10^{-16}\ \text{cm}^2 \quad . \quad (8')$$

The metastable diffusion coefficient was obtained from Huggins and Cahn.[18] Presented in modified form it is given by

$$D_M = 9.55\times10^{17} T_e^{1/2}/n_n\ \text{cm}^2\,\text{sec}^{-1} \quad . \quad (24)$$

The electron thermal conductivity was obtained from Banks.[19]

$$K_e = \frac{9.72\times10^{-16} T_e^{5/2}}{1+3.22\times10^{-12} T_e^2 n_n/n_e}\ \text{erg}\,\text{sec}^{-1}\,\text{cm}^{-1}\,\text{deg}^{-1} \quad (25)$$

The relation between K_i and K_e is from Kaufman.[20]

$$K_i = 1.37(m_e/m_n)^{1/2}(T_i/T_e)^{5/2}K_e \quad . \quad (26)$$

The neutral helium thermal conductivity is from Collins *et al.*[21]

$$K_n = 280 T_n^{0.7}\ \text{erg}\,\text{sec}^{-1}\,\text{cm}^{-1}\,\text{deg}^{-1} \quad . \quad (27)$$

The electron-ion relaxation time is from Spitzer.[22] We have used $\ln\Lambda = 3.9$.

$$\tau_{ei} = (1.01\times10^3/\ln\Lambda) T_e^{3/2}/n_e\ \text{sec} \quad . \quad (28)$$

The rates of momentum and energy transport which were used are as follows:

$$\vec{P}_{en} = \left(\frac{2.55kT_e}{m_e}\right)^{1/2} m_e\sigma_{en} n_e n_n(\vec{v}_n - \vec{v}_e) \quad , \quad (29)$$

$$\vec{P}_{in} = \left(\frac{2.55k(T_i+T_n)}{m_n}\right)^{1/2} n_n\sigma_{in} m_n n_e(\vec{v}_n - \vec{v}_e) \quad , \quad (30)$$

$$R_{en} = -4k(T_e - T_n)\frac{m_e}{m_n}\sigma_{en} n_e n_n\left(\frac{2.55kT_e}{m_e}\right)^{1/2} \quad , \quad (31)$$

$$R_{ei} = -1.5k(T_e - T_i)n_e/\tau_{ei} \quad , \quad (32)$$

$$R_{in} = -1.5k(T_i - T_n)\sigma_{in} n_e n_n\left(\frac{2.55k(T_i+T_n)}{m_n}\right)^{1/2} \quad . \quad (33)$$

APPENDIX B: THE DIFFUSION APPROXIMATION

It is common practice in solutions of the type obtained in this paper to apply "diffusion approximations" for the electrons and ions which negates the necessity of including momentum conservation equations for these two species. This approach was not taken here because in principle it can lead to considerable error in regions of steep gradients such as near the walls of the container. The "diffusion approximation" can be obtained from the momentum conservation equations (15) and (16) which reduce to the following with the aid of Eqs. (9) and (10):

$$m_e n_e\frac{\partial\vec{v}_e}{\partial t} + m_e n_e\vec{v}_e\cdot\nabla\vec{v}_e = -\nabla p_e + \vec{P}_{ei} + \vec{P}_{en} - en_e\vec{E} + m_e\beta n_{3m}{}^2(\vec{v}_{3m} - \vec{v}_e) \quad , \quad (34)$$

$$m_i n_e\frac{\partial\vec{v}_e}{\partial t} + m_i n_e\vec{v}_e\cdot\nabla\vec{v}_e = -\nabla p_i + \vec{P}_{ei} + \vec{P}_{in} + en_e\vec{E} + m_i\beta n_{3m}{}^2(\vec{v}_{3m} - \vec{v}_e) \quad . \quad (35)$$

The viscosity terms $\nabla\cdot\overleftrightarrow{\pi}_e$ and $\nabla\cdot\overleftrightarrow{\pi}_i$ have been neglected. The sum of these two equations yields

$$-\vec{P}_{en}-\vec{P}_{in}=-\nabla(p_e+p_i)-m_n n_e\frac{\partial\vec{v}_e}{\partial t}$$
$$-m_n n_e\vec{v}_e\cdot\nabla\vec{v}_e+m_n\beta n_{3m}{}^2(\vec{v}_{3m}-\vec{v}_e)\ . \quad (36)$$

Substitution of the expressions for $\vec{P}_{en}$ and $\vec{P}_{in}$ as given by Eqs. (29) and (30) and solving for $n_e(\vec{v}_e-\vec{v}_n)$ yields

$$n_e(\vec{v}_e-\vec{v}_n)=-k^{1/2}[(T_e+T_i)\nabla n_e+n_e\nabla(T_e+T_i)]$$
$$\times\{n_n(2.55)^{1/2}[(m_eT_e)^{1/2}\sigma_{en}+m_n{}^{1/2}(T_i+T_n)^{1/2}\sigma_{in}]\}^{-1}\ , \quad (37)$$

if for the present the last three terms in Eqs. 36 are neglected. The coefficient of ∇n_e is the ambipolar diffusion coefficient which is very nearly the same as that derived from kinetic theory, and agrees to within a few percent of the experimentally determined value.[23]

Equation (37) is the "diffusion approximation" to the convective flow. The main assumption involved with its use is that the last three terms in Eq. 36 can be neglected. Very little can be said about the term due to metastable-metastable collisions, except that in the plasma investigated in this work, this term could have been neglected. Order of magnitude comparison of the terms indicates that in many plasmas the other two terms are also negligible. Consider,

$$\frac{m_e n_e\vec{v}_e\cdot\nabla\vec{v}_e}{\nabla(n_ekT_e)}\sim\left(\frac{m_e n_e|\vec{v}_e|^2/L}{kT_e n_e/L}\right)\sim\frac{|\vec{v}_e|^2}{\langle v^2\rangle}$$

and

$$\frac{|P_{en}|}{m_e n_e|\partial\vec{v}_e/\partial t|}\sim\frac{\nu_{en}n_e m_e|\vec{v}_e|}{m_e n_e|\vec{v}_e|/\tau}=\nu_{en}\tau\ ,$$

where L is a characteristic size of the container, τ is the characteristic decay time for $\vec{v}_e$, and ν_{en} is the average electron-neutral collision frequency for momentum transfer. Typically,

$$\nu_{en}\tau\gg 1,\ \text{and}\ |v_e|^2/\langle v^2\rangle\ll 1\ ,$$

from which it follows that both the gradient and time derivative terms of $\vec{v}_e$ can be neglected in Eq. 36. However, these terms may not be negligible in regions where there are steep spatial gradients of $\vec{v}_e$ or during time intervals when $\vec{v}_e$ is changing rapidly.

It is interesting to note that for the plasma studied here, solution of the set of equations using the "diffusion approximation" yielded results nearly the same as those obtained using the full momentum conservation equations. The validity of the "diffusion approximation" in this particular example is of only academic interest because its applicability was realized *a posteriori*.

APPENDIX C: THE EFFECTS OF DIFFERENT TUBE DIAMETERS

The main effect of using a larger diameter tube is to reduce thermal conduction losses. The result is that temperatures and thus the electron density decays more slowly. Conversely, a smaller tube results in shorter decay times. Changing the tube size also has a quantitative effect on the relative importance of the various processes in the electron decay. For example, using a tube with twice the diameter results in, at $t=120$ μsec,

$$\alpha n_e{}^2:\beta n_{3m}{}^2:\nabla\cdot n_e\vec{v}_e=80:36:2$$

instead of the 13:9:2 of Fig. 6. In a larger tube, gradients are smaller and thus conduction and convection terms are relatively less important. Table V illustrates the importance of the tube diameter in determination of the decay.

---

*This work was supported by the United States Atomic Energy Commission.

[1]E. P. Gray and D. E. Kerr, Ann. Phys. 17, 276 (1962).

[2]J. B. Gerardo and M. A. Gusinow, J. Appl. Phys. (to be published).

[3]Gunthard K. Born and Rudolf G. Buser, J. Appl. Phys. 37, 4918 (1966).

[4]M. A. Gusinow, J. B. Gerardo, and J. T. Verdeyen, Phys. Rev. 149, 91 (1966).

[5]J. C. Ingraham and S. C. Brown, Phys. Rev. 138, A1015 (1965).

[6]Compare, e.g., G. W. Sutton and A. Sherman, Engineering Magnetohydrodynamics (McGraw-Hill, New York, 1965), p. 118, Eq. 4.173.

[7]*Ibid.*, 114 and 119.

[8]Bruce McCarroll and Gert E. Ehrlich, J. Chem. Phys. 38, 523 (1963).

[9]D. C. Montgomery and D. A. Tidman, Plasma Kinetic Theory (McGraw-Hill, New York, 1964), p. 37.

[10]D. J. T. Morrison and M. R. H. Rudge, Proc. Phys. Soc. (London) 91, 565 (1967).

[11]D. R. Bates, A. E. Kingston, and R. W. P. McWhirter, Proc. Phys. Soc. (London) 83, 43 (1964).

[12]E. Hinnov and J. G. Hirschberg, Phys. Rev. 125, 795 (1962).

[13]A. V. Phelps and J. P. Molnar, Phys. Rev. 89, 1202 (1953).

[14]R. Marriott, Proc. Phys. Soc. 87, 407 (1966).
[15]A. V. Phelps, Phys. Rev. 99, 1307 (1955).
[16]S. C. Brown, Basic Data of Plasma Physics, 1966 (MIT Press, Cambridge, Mass., 1967), p. 57.
[17]*Ibid.*, p. 17.
[18]R. W. Huggins and J. H. Cahn, J. Appl. Phys. 38, 180 (1967).
[19]P. M. Banks, Ann. Geophys. 22, 577 (1966).
[20]A. N. Kaufman, in Plasma Physics in Theory and Application, edited by W. B. Kunkel (McGraw-Hill Book Company, New York, 1966), p. 113.
[21]D. J. Collins, R. Greif, and A. E. Bryson, Jr., Intern. J. Heat Mass Transfer 8, 1209 (1965).
[22]L. Spitzer, Jr., Physics of Fully Ionized Gases (Interscience Publishers, Inc., New York, 1962), p. 135
[23]M. A. Biondi and S. C. Brown, Phys. Rev. 75, 1700 (1949).

PHYSICAL REVIEW VOLUME 179, NUMBER 1 5 MARCH 1969

Spectroscopic Measurement of High-Frequency Electric Fields in a Plasma by Observation of Two-Quantum Transitions and Spectral Line Shifts*

William S. Cooper III and Heinz Ringler†
Lawrence Radiation Laboratory, University of California, Berkeley, California 94720
(Received 3 October 1968)

We have observed normally forbidden two-quantum transitions in the optical spectrum of a helium plasma. We induced these transitions by applying a microwave field to a separately generated steady-state helium discharge. Measurements of the relative intensity and wavelength of the optical photons emitted in the two-quantum transition $5^1F^0 \rightarrow 2^1P^0$ in He I determined both the frequency and the strength of the microwave field in the plasma. The field strength was also measured by observation of the Stark shift of a spectral line and by measurement of the microwave power input and the Q of the microwave cavity. All measurements of the field strength are in satisfactory agreement and indicate an rms microwave field strength in the plasma of about 215 V/cm. The spectroscopic measurement of the frequency of the microwave field is within 3% of the actual value, and the measured polarization of the radiation agrees with theory.

I. INTRODUCTION

An oscillating electric field has certain observable effects on the spectrum of radiation emitted by excited atoms. These effects can, in principle, be used to measure the frequency, strength, and direction of the electric field. If the radiating atoms are located in a plasma, these effects provide the important possibility of studying the electric fields in the plasma by spectroscopic techniques. Two advantages of spectroscopic methods are obvious: first, the plasma is not perturbed by the measurement, and second, the frequency response is sufficient to observe even the most rapid plasma phenomena. The disadvantages are first, that it is difficult to localize the measurement unless the plasma is cylindrically symmetric, so that one may use Abel inversion,[1] and second, fairly strong fields may be required to produce measurable effects.

The theory of the linear Stark effect in a rapidly varying electric field has been discussed by Schrödinger,[2] and by Blochinzew[3] for the particular case of a sinusoidally varying electric field. The effect on a spectral line which exhibits a linear Stark effect is a modification of the line profile which, if competing line-broadening mechanisms are not too large, may be used to measure the strength and, in some cases, the frequency of the perturbing electric field. This technique has been used to measure the strength of an externally applied microwave field in a plasma[4] and to measure the strength of stochastic fields in a beam-plasma interaction experiment.[5] Both experiments were in hydrogen, and in neither case was information about the frequency spectrum of the fields derived from the measurements.

In nonhydrogenic atoms, a sinusoidally varying electric field can induce normally forbidden two-quantum transitions involving emission or absorption of one quantum from the field plus emission of an optical photon. This effect was proposed by